

Quantum kicks near a Cauchy horizon

Cite as: AVS Quantum Sci. 4, 013201 (2022); <https://doi.org/10.1116/5.0073373>

Submitted: 29 September 2021 • Accepted: 11 January 2022 • Published Online: 14 February 2022

Published open access through an agreement with JISC Collections

 Benito A. Juárez-Aubry and  Jorma Louko

COLLECTIONS

Paper published as part of the special topic on [Celebrating Sir Roger Penrose's Nobel Prize](#)



View Online



Export Citation




Submit Today!

AVS Quantum Science

Special Topic: Dark Matter Detection with Quantum Materials and Devices

Quantum kicks near a Cauchy horizon

Cite as: AVS Quantum Sci. 4, 013201 (2022); doi: 10.1116/5.0073373

Submitted: 29 September 2021 · Accepted: 11 January 2022 ·

Published Online: 14 February 2022



View Online



Export Citation



CrossMark

Benito A. Juárez-Aubry^{1,2,a),b)}  and Jorma Louko^{2,a)} 

AFFILIATIONS

¹Instituto de Ciencias Nucleares, Universidad Nacional Autónoma de México, Mexico City 045010, Mexico

²School of Mathematical Sciences, University of Nottingham, Nottingham NG7 2RD, United Kingdom

Note: This paper is part of the special topic Celebrating Sir Roger Penrose's Nobel Prize.

^{a)}Electronic addresses: benito.juarez@correo.nucleares.unam.mx and jorma.louko@nottingham.ac.uk

^{b)}Present address: Instituto de Ciencias Nucleares, Universidad Nacional Autónoma de México, Mexico City 045010, Mexico.

ABSTRACT

We analyze a quantum observer who falls geodesically toward the Cauchy horizon of a $(1 + 1)$ -dimensional eternal black hole spacetime with the global structure of the non-extremal Reissner–Nordström solution. The observer interacts with a massless scalar field, using an Unruh–DeWitt detector coupled linearly to the proper time derivative of the field, and by measuring the local energy density of the field. Taking the field to be initially prepared in the Hartle–Hawking–Israel (HHI) state or the Unruh state, we find that both the detector's transition rate and the local energy density generically diverge on approaching the Cauchy horizon, respectively, proportionally to the inverse and the inverse square of the proper time to the horizon, and in the Unruh state the divergences on approaching one of the branches of the Cauchy horizon are independent of the surface gravities. When the outer and inner horizons have equal surface gravities, the divergences disappear altogether in the HHI state and for one of the Cauchy horizon branches in the Unruh state. We conjecture, on grounds of comparison with the Rindler state in $1 + 1$ and $3 + 1$ Minkowski spacetimes, that similar properties hold in $3 + 1$ dimensions for a detector coupled linearly to the quantum field, but with a logarithmic rather than inverse power-law divergence.

© 2022 Author(s). All article content, except where otherwise noted, is licensed under a Creative Commons Attribution (CC BY) license (<http://creativecommons.org/licenses/by/4.0/>). <https://doi.org/10.1116/5.0073373>

I. INTRODUCTION

It is a great pleasure to dedicate this paper to Roger Penrose, who realized the instability of the Cauchy horizons that occur inside charged and rotating black hole solutions.¹ The nature of the instability is a topic of ongoing research, classically and in the presence of quantized fields. This paper addresses transitions in a time-and-space localized quantum system, coupled to an ambient quantum field, when the system falls geodesically toward a Cauchy horizon.

Causality is a concept at the core of physics. Classically, causality is formulated as the well-posedness of the initial value problem: a solution to the dynamical equations is fully determined by the initial conditions specified on a spacelike hypersurface. In quantum theory, causality may be formulated in terms of an algebra of observables: The commutator of two observables whose respective supports have spacelike separation must vanish. In both cases, the physical meaning is that any two causally disconnected observables have no influence on each other.

In geometric terms, causality is protected by global hyperbolicity.^{2,3} Every globally hyperbolic spacetime is stably causal, since global hyperbolicity implies the existence of a global time function that

provides the stable causality condition. In turn, this implies strong causality, which prevents any causal curve from coming arbitrarily close to intersecting itself. Moreover, the dynamical equations of classical fields admit a well-posed initial value problem on the whole manifold whenever suitable data are specified on a Cauchy hypersurface of a globally hyperbolic manifold. With quantum fields, global hyperbolicity allows one to establish a rigorous quantization scheme for free fields,^{4,5} which provides the starting point for a perturbative expansion in interacting theories.⁶

However, many important solutions in General Relativity are not globally hyperbolic: They contain Cauchy horizons, which are boundaries of the maximal Cauchy development of an achronal hypersurface. This includes most members of the analytically extended Kerr–Newman family.

There is a significant history of work addressing the stability of Cauchy horizons in General Relativity. In the classical theory, work by Simpson and Penrose led to the *strong cosmic censorship conjecture*,¹ which states that for generic initial data the spacetime is inextendible beyond the maximal Cauchy development. Support for this conjecture came from Chandrasekhar and Hartle's observation that the

(electromagnetic or gravitational) classical radiation felt by an observer diverges as the Reissner–Nordström horizon is approached.⁷ Later work has however revealed that the sense of inextendibility in the conjecture is subtle. On the one hand, given polynomially decaying initial data for the Einstein–Maxwell–scalar system, settling down to a Reissner–Nordström black hole, the spacetime is C^0 -extendible past the Cauchy horizon; on the other hand, not all the geometric invariants remain finite and, in particular, the Hawking mass diverges at the Cauchy horizon. This is known as the mass inflation scenario.^{8–12}

When the theory is extended to include quantized fields, new issues arise from the renormalized stress-energy tensor near the Cauchy horizon, and from the back-reaction of this stress-energy on the spacetime. There is evidence that the back-reaction of the quantum fields tends to make Cauchy horizons generically unstable even in situations where classical surface gravity considerations would suggest stability.^{13–17}

In this paper, we shall address another facet of the singular behavior of quantized fields near a Cauchy horizon: the experiences of a time-and-space localized quantum system as it falls geodesically toward the Cauchy horizon. Interaction with the ambient quantum field causes transitions between the internal states of the localized quantum system. Does the probability of these transitions change rapidly, perhaps even divergently, as the system approaches the Cauchy horizon? If so, is there a correlation between the rapid changes in transition probabilities and any divergent behavior that the field’s stress-energy tensor may exhibit near the Cauchy horizon?

We shall consider a class of $(1+1)$ -dimensional eternal black hole spacetimes whose global structure mimics that of the non-extremal Reissner–Nordström solution, with an asymptotically flat region, an outer bifurcate Killing horizon, and an inner bifurcate Killing horizon,² but allowing the “radial” profile function in the metric to remain otherwise arbitrary, and in particular allowing the outer and inner horizons to have arbitrary nonvanishing surface gravities. As the ambient quantum field, we consider a massless scalar field, prepared initially in the Hartle–Hawking–Israel (HHI) state^{18,19} or in the Unruh state.²⁰ As the local quantum system, we consider a spatially pointlike two-level system known as the Unruh–DeWitt (UDW) detector,^{20,21} in a variant that couples linearly to the proper time derivative of the field. The reason to include the derivative is that this makes the detector’s transition probabilities independent of the scalar field’s infrared ambiguity.

We work within first-order perturbation theory. We assume the detector to be switched on and off instantaneously, and we address not the transition probability itself but the transition rate, defined as the derivative of the transition probability with respect to the switch-off proper time. While this amounts to ignoring a technically divergent “additive constant” contribution to the transition probability from the instantaneous switching,^{22–27} it allows us to isolate the singular effects due to the approach to the Cauchy horizon, which effects are the focus of this paper.

We find that as the geodesic detector approaches the Cauchy horizon, the transition rate diverges whenever the outer and inner horizons have differing surface gravities, on all parts of the Cauchy horizon. In the exceptional case of equal surface gravities, the transition rate remains bounded in the HHI state on all parts of the Cauchy horizon, and in the Unruh state on the branch of the Cauchy horizon that is opposite to the exterior with respect to which the Unruh state is

defined. When the divergence occurs, it is proportional to the inverse of the proper time separation from the Cauchy horizon, except that in the Unruh state, for a geodesic approaching the Cauchy horizon bifurcation point, the divergence is slightly weaker when the outer horizon has twice the surface gravity of the inner horizon.

We also find that these results for the transition rate are in significant qualitative and quantitative agreement with the divergences in the energy density seen by an observer on the geodesics. The main difference is that the energy density generically diverges proportionally to the inverse square, rather than the inverse, of the proper time separation from the Cauchy horizon; however, in the energy density averaged over the trajectory, the divergence is again proportional to the inverse of the proper time separation from the Cauchy horizon. The divergence in the stress-energy tensor, including the special role of the equal surface gravity case therein, has been studied in the context of back-reaction, in both $1+1$ dimensions and in $3+1$ dimensions.^{15–17}

Finally, we perform a similar analysis for a geodesic detector approaching the Rindler horizon in $(1+1)$ -dimensional Minkowski spacetime, with the field prepared in the Rindler vacuum, and we contrast the results with a similar analysis in $3+1$ dimensions,²⁶ for a detector coupled linearly to the value (as opposed to the derivative) of the scalar field. Based on this comparison, we conjecture that in $3+1$ spacetime dimensions, a detector coupled linearly to the value of the scalar field, and approaching a Cauchy horizon, generically has a transition rate that diverges in proper time but only logarithmically.

We begin in Sec. II by presenting our $(1+1)$ -dimensional eternal black hole spacetime, discussing its similarities with the $(3+1)$ -dimensional non-extremal Reissner–Nordström solution, presenting adapted coordinate systems, and recording properties of timelike geodesics that approach the Cauchy horizon. Section III introduces the massless scalar field and records its Wightman functions in the HHI and Unruh states. Section IV starts with a concise conceptual review of Unruh–DeWitt detectors as space-and-time localized quantum systems by which the quantum field is probed, specializes then to a detector whose coupling to the field includes a time derivative, and focuses finally on the detector’s instantaneous transition rate, treated in first-order perturbation theory.

Our main results, for the detector’s transition rate on approaching the Cauchy horizon, are presented in Sec. V, deferring technical aspects to three appendixes. Section VI presents the corresponding results for the energy density on a geodesic, and Sec. VII presents a comparison with the Rindler horizon, in $1+1$ and $3+1$ dimensions. Section VIII gives a summary and concluding remarks.

We use units in which $c = \hbar = k_B = 1$. In asymptotic expansions, $\mathcal{O}(x)$ denotes a quantity such that $\mathcal{O}(x)/x$ is bounded as $x \rightarrow 0$, $o(x)$ denotes a quantity such that $o(x)/x \rightarrow 0$ as $x \rightarrow 0$, $\mathcal{O}(1)$ denotes a quantity that is bounded in the limit under consideration, and $o(1)$ denotes a quantity that goes to zero in the limit under consideration.

A subset of our results was announced previously in a conference proceedings contribution.²⁸ The key result given therein as formula (3.10), for the transition rate of a detector approaching the “left” branch of the Cauchy horizon when the field is in the HHI state, is our formula (5.3a). The formulas have the same content, given the differing surface gravity conventions: In the present paper, the surface gravities of both inner and outer horizons are by definition positive, following the conventions of Refs. 15–17, whereas in Ref. 28 the inner

horizon surface gravity was defined to be negative. For the stress-energy, the present paper focuses on the energy density at a given moment on the trajectory, allowing a sharper asymptotic localization than the time-averaged energy density discussed in Sec. 4 of Ref. 28.

II. THE GENERALIZED REISSNER-NORDSTRÖM BLACK HOLE IN 1 + 1 DIMENSIONS

In this section, we introduce a class of (1 + 1)-dimensional eternal black hole spacetimes that generalize the constant angles sections of the non-extremal Reissner-Nordström spacetime. We also write down the equations of geodesics approaching the Cauchy horizon in a convenient form.

A. Metric and global structure

Let $F : \mathbb{R}^+ \rightarrow \mathbb{R}$ be a smooth function such that

$$F(r_-) = F(r_+) = 0, \tag{2.1}$$

where r_{\pm} are constants satisfying $0 < r_- < r_+$,

$$F(r) > 0 \quad \text{for } r_+ < r < \infty, \tag{2.2a}$$

$$F(r) < 0 \quad \text{for } r_- < r < r_+, \tag{2.2b}$$

and

$$F'(r_+) = 2\kappa_+ > 0, \tag{2.3a}$$

$$F'(r_-) = -2\kappa_- < 0, \tag{2.3b}$$

where κ_{\pm} are positive constants. We also assume that $F(r) \rightarrow 1$ as $r \rightarrow \infty$. Further information about $F(r)$ for $r < r_-$ will not be needed, but we note that it follows from the above that $F(r) > 0$ when $r \in (a, r_-)$ for some $a < r_-$.

To summarize, $F(r) \rightarrow 1$ as $r \rightarrow \infty$, and F has simple zeroes at $r = r_{\pm}$.

We consider the spacetime metric

$$ds^2 = -F(r)dt^2 + \frac{dr^2}{F(r)}, \tag{2.4}$$

where, to begin with, $r > r_+$. We refer to (t, r) as Schwarzschild-like coordinates. This metric is static, with the timelike Killing vector $\xi \doteq \partial_t$, and it is asymptotically flat at $r \rightarrow \infty$.

The metric has a smooth continuation across the coordinate singularity at $r = r_+$, and further a smooth continuation across the coordinate singularity at $r = r_-$. These continuations may be found by adapting the standard procedure for the Reissner-Nordström metric,² for which $F(r) = (r - r_+)(r - r_-)/r^2$, and the continuations are real analytic when F is real analytic. There is a bifurcate Killing horizon of ξ at $r = r_+$, of surface gravity κ_+ , and part of this Killing horizon forms the black hole event horizon with respect to the \mathcal{S}^+ of the original asymptotically flat region. On continuing to the past and to the future, there are further bifurcate Killing horizons of ξ at $r = r_-$, of surface gravity κ_- , and they form past and future Cauchy horizons for the four regions joined by the original $r = r_+$ Killing horizon. The pattern continues to the past and to the future. What happens at $r < r_-$ depends on the behavior of $F(r)$ there, and will not be needed here. The parts of the conformal diagram that are relevant for us are shown in Fig. 1, in the Reissner-Nordström-like case in which $F(r) > 0$ for $r < r_-$ and $F(r) \rightarrow \infty$ as $r \rightarrow 0$.

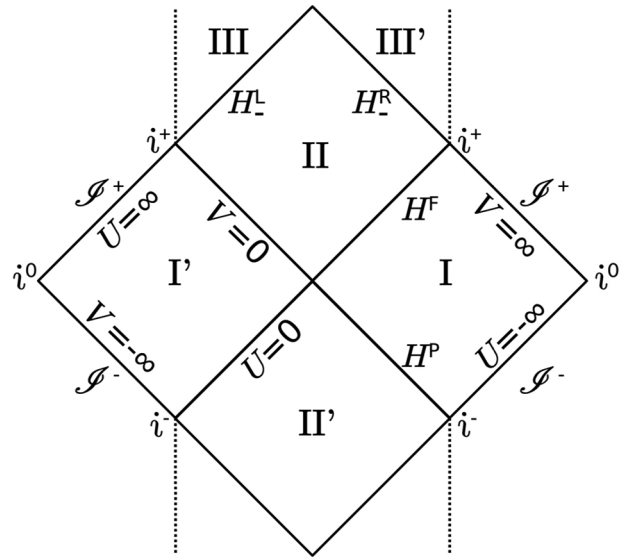


Fig. 1. Part of the conformal diagram of the extended spacetime. Region I is the original exterior (2.4), connected by the bifurcate Killing horizon at $r = r_+$ to the black hole interior II, the white hole interior II' and the second exterior I'. The Kruskal-like coordinates (U, V) cover regions I, II, II', and I', with the Killing horizon $r = r_+$ at $UV = 0$. Regions II and II' are bounded in the future/past by the future/past Cauchy horizons at $r = r_-$. The dotted lines, bounding regions III and III', are singularities that occur behind the Cauchy horizons when $F(r) > 0$ for $r < r_-$ and $F(r) \rightarrow \infty$ as $r \rightarrow 0$; other structure behind the Cauchy horizons can occur under different behavior of $F(r)$ for $r < r_-$. The diagram extends to the past and future.

B. Coordinates

We shall write down three coordinate systems that cover (at least) the original exterior region and the black hole interior region, and are adapted to the quantum states that we shall describe in Sec. III.

1. Kruskal-like coordinates

We denote the “original” $r > r_+$ region of (2.4) by region I. In region I, define first the tortoise coordinate $r_* \in \mathbb{R}$ by

$$dr_* = \frac{dr}{F(r)}, \tag{2.5}$$

making some arbitrary choice for the additive constant in r_* , and then the Eddington-Finkelstein double null coordinates $(u, v) \in \mathbb{R}^2$ by

$$u = t - r_*, \tag{2.6a}$$

$$v = t + r_*, \tag{2.6b}$$

and finally the Kruskal(-Szekeres)-like coordinates $(U, V) \in \mathbb{R}^- \times \mathbb{R}^+$ by

$$U = -e^{-\kappa_+ u}, \tag{2.7a}$$

$$V = e^{\kappa_+ v}. \tag{2.7b}$$

The metric takes the form

$$ds^2 = \frac{F(r)}{\kappa_+^2 UV} dU dV, \tag{2.8}$$

where r is determined as a function of U and V from

$$-UV = e^{2\kappa_+ r_*}. \tag{2.9}$$

It follows from the assumptions about F that the metric given by (2.8) with (2.9) can be smoothly extended from region I, where $(U, V) \in \mathbb{R}^- \times \mathbb{R}^+$, to $(U, V) \in \mathbb{R} \times \mathbb{R}$, as summarized in Table I and illustrated in Fig. 1: The extension covers regions I, II, II', and I' as shown in Fig. 1, and the boundaries at which they are joined. We call this spacetime \mathcal{M}_K . In regions II and II', where $UV > 0$, $r \in (r_-, r_+)$ is determined as a function of U and V from

$$UV = e^{2\kappa_+ \tilde{r}_*}, \tag{2.10}$$

where the relation between r and \tilde{r}_* is determined by

$$d\tilde{r}_* = \frac{dr}{F(r)}, \tag{2.11}$$

with the additive constant in \tilde{r}_* chosen so that the extension of the metric function $F(r)(\kappa_+^2 UV)^{-1}$ in (2.8) across $UV=0$ is smooth. If F is real analytic, the extended metric is real analytic. Note that ζ extends smoothly from region I to \mathcal{M}_K , having the formula $\zeta = \kappa_+(-U\partial_U + V\partial_V)$, and ζ has a bifurcate Killing horizon at $UV=0$, where $r = r_+$.

The coordinates (U, V) do not extend to $r = r_-$. Another set of Kruskal-type coordinates can be introduced to cover the four regions joined at the Killing horizon $r = r_-$; these coordinates will however not be needed for what follows.

2. Hybrid coordinates

Consider the region where $-\infty < U < \infty$ and $0 < V < \infty$. In Fig. 1, this consists of regions I and II and their joint boundary, the black hole horizon H^F . We call this spacetime \mathcal{M}_U .

Given the Kruskal-like coordinates $(U, V) \in \mathbb{R} \times \mathbb{R}^+$ in \mathcal{M}_U , we introduce the new coordinates $(U, v) \in \mathbb{R} \times \mathbb{R}$ in \mathcal{M}_U by (2.7b). We refer to these as the hybrid coordinates, being Kruskal-like in U and Eddington–Finkelstein-like in v . The metric takes the form

$$ds^2 = \frac{F(r)}{\kappa_+ \tilde{U}} dU dv, \tag{2.12}$$

where r is determined as a function of U and v from

$$-Ue^{\kappa_+ v} = e^{2\kappa_+ r_*} \text{ for } U < 0, \tag{2.13a}$$

$$Ue^{\kappa_+ v} = e^{2\kappa_+ \tilde{r}_*} \text{ for } U > 0, \tag{2.13b}$$

with r related to r_* and \tilde{r}_* as above. The black hole horizon H^F is at $U=0$.

TABLE I. The four subregions of the Kruskal-type chart (U, V) , in the labeling of Fig. 1. The last three columns indicate the signs of U , V , and $\zeta_a \zeta^a$ in each of the subregions.

Region	r domain	U	V	$\zeta_a \zeta^a$
I	Original exterior	$r_+ < r < \infty$	-	+
II	Black hole	$r_- < r < r_+$	+	+
II'	White hole	$r_- < r < r_+$	-	+
I'	Second exterior	$r_+ < r < \infty$	+	-

3. Eddington–Finkelstein coordinates

For completeness, we record here how the standard ingoing Eddington–Finkelstein coordinates are related to the coordinate systems introduced above.

In \mathcal{M}_U , starting from (2.12) and replacing U by r puts the metric in the Eddington–Finkelstein form

$$ds^2 = -F(r)dv^2 + 2dv dr, \tag{2.14}$$

where $r_- < r < \infty$ and $v \in \mathbb{R}$. This metric can be extended to $0 < r < \infty$, covering also H_-^F and region III in Fig. 1. The usual way to obtain (2.14) is to start from region I with the metric (2.4), set $dt = dv - dr/F(r)$, and then allow $0 < r < \infty$.

C. Timelike geodesics approaching the Cauchy horizon

We are interested in timelike geodesics in the black hole interior, region II in Fig. 1.

It is convenient to introduce in region II the interior Schwarzschild-like coordinates (\tilde{t}, r) , in which the metric reads

$$ds^2 = \frac{dr^2}{F(r)} - F(r)d\tilde{t}^2, \tag{2.15}$$

where now $F(r) < 0$, $r \in (r_-, r_+)$ is a timelike coordinate decreasing to the future, and $\tilde{t} \in \mathbb{R}$ is a spacelike coordinate increasing to the right. These coordinates may be obtained from (2.14) by writing $dv = d\tilde{t} + dr/F(r)$, or from (2.8) by writing first

$$U = e^{\kappa_+ \tilde{u}}, \tag{2.16a}$$

$$V = e^{\kappa_+ \tilde{v}}, \tag{2.16b}$$

where $(U, V) \in \mathbb{R}_+ \times \mathbb{R}_+$ and $(\tilde{u}, \tilde{v}) \in \mathbb{R} \times \mathbb{R}$, and then

$$\tilde{u} = \tilde{r}_* - \tilde{t}, \tag{2.17a}$$

$$\tilde{v} = \tilde{r}_* + \tilde{t}, \tag{2.17b}$$

and finally using (2.11) to replace \tilde{r}_* by r .

From (2.15), it is now straightforward to verify that the timelike geodesics are the integral curves of the system

$$\dot{\tilde{t}} = \frac{E}{F(r)}, \tag{2.18a}$$

$$\dot{r} = -\sqrt{E^2 - F(r)}, \tag{2.18b}$$

where the overdot denotes derivative with respect to the proper time, increasing to the future, and $E \in \mathbb{R}$ is a constant of integration. In the coordinates (\tilde{u}, \tilde{v}) , the system (2.18) reads

$$\dot{\tilde{u}} = \frac{1}{\sqrt{E^2 - F(r)} - E}, \tag{2.19a}$$

$$\dot{\tilde{v}} = \frac{1}{\sqrt{E^2 - F(r)} + E}. \tag{2.19b}$$

All these geodesics hit the Cauchy horizon at $r = r_-$ in finite proper time. A geodesic with $E > 0$ travels toward decreasing \tilde{t} , crossing the Cauchy horizon's left branch H_-^L into region III, as is perhaps most easily seen in the Eddington–Finkelstein coordinates (2.14); similarly, a geodesic with $E < 0$ travels toward increasing \tilde{t} , crossing the

Cauchy horizon's right branch H^R into region III'. A geodesic with $E=0$ crosses the bifurcation point where H^L and H^R meet, entering a new region in which $r \in (r_-, r_+)$.

We note that a geodesic with $E>0$ continues in the past to region I, having fallen in from there, a geodesic with $E<0$ has fallen in from region I', and a geodesic with $E=0$ has emerged from region II', the white hole, through the bifurcation point where regions I, I', II, and II' meet. We shall however not consider these geodesics beyond region II, in the past or in the future.

III. QUANTUM SCALAR FIELD

Let ϕ be a real massless scalar field, with the field equation

$$\square\phi = 0. \tag{3.1}$$

In \mathcal{M}_K , it follows from the conformal invariance of the massless scalar field, and the conformally flat form of the metric given in (2.8), that ϕ has a Fock quantization based on the input encoded in the Kruskal coordinates. The field equation reads

$$\partial_U\partial_V\phi = 0, \tag{3.2}$$

and a Fock quantization is obtained by defining positive frequencies in terms of ∂_U and ∂_V . The corresponding vacuum state is known as the Hartle–Hawking–Israel (HHI) state $|0_H\rangle$.^{18,19} The Wightman function in $|0_H\rangle$ is given by

$$\begin{aligned} \mathcal{W}_H(\mathbf{x}, \mathbf{x}') &\doteq \langle 0_H | \phi(\mathbf{x})\phi(\mathbf{x}') | 0_H \rangle \\ &= -\frac{1}{4\pi} \ln [(\epsilon + i\Delta U)(\epsilon + i\Delta V)], \end{aligned} \tag{3.3}$$

where we have written $\mathbf{x} = (U, V)$ and $\mathbf{x}' = (U', V')$, with $\Delta U = U - U'$ and $\Delta V = V - V'$. The logarithm denotes the branch that is real-valued for positive argument, and the limit $\epsilon \rightarrow 0_+$ is understood.

In \mathcal{M}_U , it follows from the conformally flat form of the metric given in (2.12) that ϕ has a Fock quantization based on the input encoded in the hybrid coordinates, and this quantization is inequivalent to that obtained by restriction of the above Fock quantization in \mathcal{M}_K . The field equation reads

$$\partial_U\partial_v\phi = 0, \tag{3.4}$$

and a Fock quantization is obtained by defining positive frequencies in terms of ∂_U and ∂_v . The corresponding vacuum state is known as the Unruh state $|0_U\rangle$.²⁰ The Wightman function in $|0_U\rangle$ is given by

$$\begin{aligned} \mathcal{W}_U(\mathbf{x}, \mathbf{x}') &\doteq \langle 0_U | \phi(\mathbf{x})\phi(\mathbf{x}') | 0_U \rangle \\ &= -\frac{1}{4\pi} \ln [(\epsilon + i\Delta U)(\epsilon + i\Delta v)], \end{aligned} \tag{3.5}$$

where the notation is as in (3.3) but now with $\Delta v = v - v'$. The logarithm denotes again the branch that is real-valued for positive argument, and the limit $\epsilon \rightarrow 0_+$ is understood.

$|0_H\rangle$ is by construction regular in \mathcal{M}_K and $|0_U\rangle$ is regular in \mathcal{M}_U , in the sense that the short distance behavior of both \mathcal{W}_H and \mathcal{W}_U satisfies the Hadamard condition.²⁹ Observers at constant r in region I experience $|0_H\rangle$ as a thermal equilibrium state, in the local Hawking temperature $T_H(r) = \kappa_+ / (2\pi\sqrt{F(r)})$,^{18,19} whereas these observers experience $|0_U\rangle$ as a state in which the ingoing part of the field is in a vacuum-like state but the outgoing part is in the local

Hawking temperature T_H .²⁰ $|0_U\rangle$ mimics the late-time properties of a state that ensues from the collapse of an initially static star.^{20,30,31}

Both \mathcal{W}_H and \mathcal{W}_U have an infrared ambiguity, characteristic of a massless field in 1+1 dimensions, and we have resolved this ambiguity as shown in (3.3) and (3.5). \mathcal{W}_H is invariant under the isometry generated by ξ . \mathcal{W}_U is invariant under this isometry only up to an additive constant; further, our formula (3.5) for \mathcal{W}_U contains dimensionally inconsistent notation in that U is dimensionless but v has the dimension of length. However, in the rest of the paper we shall probe \mathcal{W}_H and \mathcal{W}_U by means that involve derivatives: Under this probing, both \mathcal{W}_H and \mathcal{W}_U will give answers that are invariant under the isometry generated by ξ , and the dimensional inconsistency of (3.5) will drop out. A similar issue in the (1+1)-dimensional Schwarzschild spacetime was discussed in Refs. 27 and 31.

IV. UNRUH-DEWITT DETECTOR: TRANSITION PROBABILITY AND TRANSITION RATE

In this section, we first briefly review the technical and conceptual aspects of probing a quantum field with time-and-space localized quantum systems known as Unruh–DeWitt (UDW) detectors.^{20,21} We then specialize to a spatially pointlike detector, coupled linearly to the proper time derivative of the scalar field, and treated to first order in perturbation theory.

A. A quantum detector localized in time and space

We wish to probe the quantum field with a time-and-space localized quantum system known as an Unruh–DeWitt (UDW) detector.^{20,21} a quantum system that moves through the spacetime on the timelike worldline $\mathbf{x}(\tau)$, parametrized by the proper time τ . What needs to be specified is the detector's internal dynamics, the sense of localization, and the coupling.

For the internal dynamics, we assume that the detector is a two-level system. The Hilbert space is spanned by two orthonormal states, with the respective eigenenergies 0 and $\omega \in \mathbb{R} \setminus \{0\}$, defined with respect to τ . For $\omega > 0$, the state with eigenenergy 0 is the ground state and the state with eigenenergy ω is the excited state; for $\omega < 0$, the roles of the states are reversed.

Generalizations to detectors with multiple levels could be considered. For example, a detector that has the dynamics of a harmonic oscillator is convenient when the coupling between the field and the detector is analyzed nonperturbatively.^{32,33} Multiple-level systems however reduce to two-level systems when treated in first-order perturbation theory, and this is what we shall do below.

For the localization in space, we assume that the detector's spatial size is negligible, as in the detector model introduced by DeWitt:²¹ the detector is restricted strictly to the worldline $\mathbf{x}(\tau)$. This will make the coupling between the field and the detector slightly singular, but the singularity will not produce infinities in the first-order perturbative treatment that we shall follow below. Allowing the detector to have a nonzero spatial size, as in the detector model originally introduced by Unruh,²⁰ would present a technical challenge for formulating the notion of a spatial profile when the spacetime is curved, or even in flat spacetime when the detector's motion is non-inertial,^{22,23,34–36} further, a finite spatial size would raise questions about the relativistic consistency of the coupled system, and about the sense in which the two-level detector approximates an underlying more fundamental detection described by quantum fields.^{37–40}

For the localization in time, we assume that the detector operates for a finite interval of proper time. As we wish to consider a strongly time-dependent situation, we shall consider the limit in which the switch-on and switch-off are instantaneous. While this limit creates a divergence in the detector’s transition probability, the divergence is a pure switching effect, and the time-dependent features can be extracted by considering the transition rate, rather than the transition probability, as we shall discuss below in Sec. IV B.

For the coupling between the field and the detector, a frequently considered choice is to couple the detector linearly to $\phi(\mathbf{x}(\tau))$, that is, to the value of the field ϕ at the location of the detector: This model is known to capture the essential features of light–matter interaction when angular momentum interchange is negligible.^{41,42} In our case of a massless field in 1 + 1 spacetime dimensions, this choice however inherits the infrared ambiguity of the Wightman function. We therefore couple the detector linearly to $\partial_\tau \phi(\mathbf{x}(\tau))$, that is, to the proper time derivative of ϕ at the location of the detector, which will cure the infrared ambiguity. A selection of previous work on a derivative-coupled detector in a range of contexts is available in Refs. 27, 31, and 43–56.

Nonlinear couplings could be considered, but they would typically require additional regularization.⁵⁷ We shall consider the linear coupling to $\partial_\tau \phi(\mathbf{x}(\tau))$.

B. Spatially pointlike detector with a linear derivative coupling

To recap, we consider a spatially pointlike two-level detector, on the timelike worldline $\mathbf{x}(\tau)$, parametrized by the proper time τ , coupled linearly to $\partial_\tau \phi(\mathbf{x}(\tau))$.

Working to first-order perturbation theory in the coupling between the detector and the field, the probability of the detector to make a transition from the eigenenergy 0 state to the eigenenergy ω state is a multiple of the response function $\mathcal{F}(\omega)$, given by

$$\mathcal{F}(\omega) = \int d\tau' d\tau'' \chi(\tau') \chi(\tau'') e^{-i\omega(\tau' - \tau'')} \times \partial_{\tau'} \partial_{\tau''} \mathcal{W}(\tau', \tau''), \quad (4.1)$$

where $\mathcal{W}(\tau', \tau'') = \langle \Psi | \phi(\mathbf{x}(\tau')) \phi(\mathbf{x}(\tau'')) | \Psi \rangle$ is the pullback of the scalar field’s Wightman function to the detector’s worldline, $|\Psi\rangle$ denotes the initial state of the field, and the real-valued switching function χ specifies how the interaction is turned on and off. When $|\Psi\rangle$ is a state satisfying the Hadamard short-distance condition,²⁹ $\mathcal{W}(\tau', \tau'')$ is a well-defined distribution under mild assumptions about the detector’s trajectory,^{58,59} and $\mathcal{F}(\omega)$ is well defined under mild assumptions about χ ; for example, taking χ to be smooth and of compact support suffices. As the factor relating $\mathcal{F}(\omega)$ to the probability depends only on the detector’s internal structure, we refer to $\mathcal{F}(\omega)$ as the transition probability, with a minor abuse of terminology. Note that the derivatives in (4.1) are responsible for making the infrared ambiguity of \mathcal{W} drop out of \mathcal{F} .

The response function $\mathcal{F}(\omega)$ (4.1) depends not just on the quantum field’s initial state $|\Psi\rangle$ and the detector’s trajectory, but also on the switching function χ . To consider the response of the detector as it approaches the Cauchy horizon, we consider a χ that cuts off at a sharply defined moment of proper time, shortly before the trajectory reaches the horizon. This creates a technical issue: If the detector is switched on sharply at proper time τ_0 and off at proper time $\tau > \tau_0$, so that $\chi(u) = \Theta(\tau - u)\Theta(u - \tau_0)$, $\mathcal{F}(\omega)$ becomes divergent, due to

the large contributions from the switch-on and switch-off moments; the issue for a derivative-coupling detector in 1 + 1 dimensions is the same as for a non-derivative-coupling detector in 3 + 1 dimensions.^{22–27} To circumvent this issue, we shall not consider the sharp switching limit of the transition probability $\mathcal{F}(\omega)$, but we consider instead the transition rate, the derivative of this probability with respect to the switch-off moment, which has a finite limit when the switching becomes sharp. Denoting the transition rate by $\dot{\mathcal{F}}(\omega, \tau, \tau_0)$, where τ_0 and τ are, respectively, the switch-on and switch-off proper times, we have²⁷

$$\begin{aligned} \dot{\mathcal{F}}(\omega, \tau, \tau_0) = & -\omega \Theta(-\omega) + \frac{1}{\pi} \left(\frac{\cos(\omega \Delta\tau)}{\Delta\tau} + |\omega| \text{si}(|\omega| \Delta\tau) \right) \\ & + 2 \int_{\tau_0}^{\tau} d\tau' \text{Re} \left[e^{-i\omega(\tau - \tau')} \left(\partial_\tau \partial_{\tau'} \mathcal{W}(\tau, \tau') + \frac{1}{2\pi(\tau - \tau')^2} \right) \right], \end{aligned} \quad (4.2)$$

where $\Delta\tau \doteq \tau - \tau_0$ and si is the sine integral function.⁶⁰ Note that the integrand in (4.2) is nonsingular at $\tau' \rightarrow \tau$ because of the Hadamard property of the Wightman function.²⁹

We shall use (4.2) to address the behavior of $\dot{\mathcal{F}}(\omega, \tau, \tau_0)$ near the Cauchy horizon in Sec. V.

V. DETECTOR NEAR THE CAUCHY HORIZON

We now specialize to a detector on a geodesic in region II, as described in Sec. II C, and we specialize to the HHI and Unruh states as described in Sec. III. We shall find the leading behavior of the transition rate as the detector approaches the Cauchy horizon.

Let τ_h be the value of the proper time at which the trajectory hits the Cauchy horizon. In the notation of (4.2), we then have $\tau_0 < \tau < \tau_h$, where τ_0 is the switch-on moment and τ is the switch-off moment. For concreteness, we assume that the switch-on moment τ_0 is in region II, for all trajectories and all states. We consider the asymptotic behavior of $\dot{\mathcal{F}}(\omega, \tau, \tau_0)$ (4.2) as $\tau \rightarrow \tau_h$, with τ_0 fixed.

Note first that the terms outside the integral in (4.2) are of order $\mathcal{O}(1)$ as $\tau \rightarrow \tau_h$. Also, note that by (3.3) and (3.5), the imaginary part of $\mathcal{W}(\tau, \tau')$ is a constant for $\tau' < \tau$. We hence have

$$\begin{aligned} \dot{\mathcal{F}}(\omega, \tau, \tau_0) = & 2 \int_{\tau_0}^{\tau} d\tau' \cos(\omega(\tau - \tau')) \\ & \times \left(\partial_\tau \partial_{\tau'} \mathcal{W}(\tau, \tau') + \frac{1}{2\pi(\tau - \tau')^2} \right) + \mathcal{O}(1). \end{aligned} \quad (5.1)$$

Integrating by parts gives

$$\begin{aligned} \dot{\mathcal{F}}(\omega, \tau, \tau_0) = & -2 \cos(\omega \Delta\tau) \partial_\tau \mathcal{W}(\tau, \tau_0) \\ & + 2 \lim_{\tau' \rightarrow \tau} \left(\partial_\tau \mathcal{W}(\tau, \tau') + \frac{1}{2\pi(\tau - \tau')} \right) \\ & - 2\omega \int_{\tau_0}^{\tau} d\tau' \sin(\omega(\tau - \tau')) \left(\partial_\tau \mathcal{W}(\tau, \tau') + \frac{1}{2\pi(\tau - \tau')} \right) \\ & + \mathcal{O}(1), \end{aligned} \quad (5.2)$$

where the second term on the right-hand side is well defined and finite by the Hadamard property of the state.²⁹

What remains is to estimate (5.2) as $\tau \rightarrow \tau_h$, for the HHI and Unruh states, and for a detector approaching the Cauchy horizon on the left branch H_-^L , on the right branch H_-^R , and at the bifurcation

point. We address the three different parts of the Cauchy horizon in, respectively, [Appendixes A, B, and C](#). We collect the outcomes here.

In the HHI state, we find

$$\dot{\mathcal{F}}_H^L(\omega, \tau, \tau_0) = \dot{\mathcal{F}}_H^R(\omega, \tau, \tau_0) = \frac{1}{4\pi(\tau_h - \tau)} \left(\frac{\kappa_+}{\kappa_-} - 1 + o(1) \right), \quad (5.3a)$$

$$\dot{\mathcal{F}}_H^0(\omega, \tau, \tau_0) = \frac{1}{2\pi(\tau_h - \tau)} \left(\frac{\kappa_+}{\kappa_-} - 1 + o(1) \right), \quad (5.3b)$$

where the superscripts L , R , and 0 indicate, respectively, H_-^L , H_-^R , and the bifurcation point. When $\kappa_+ \neq \kappa_-$, the leading term hence diverges proportionally to $1/(\tau_h - \tau)$, in all three cases, with an overall sign that differs for $\kappa_- < \kappa_+$ and $\kappa_+ < \kappa_-$. That the responses on approaching H_-^L and H_-^R are identical follows from the left–right symmetry of the HHI state, and the divergence for H_-^L (respectively, H_-^R) comes only from the right-moving (respectively, left-moving) part of the field. The divergence on approaching the bifurcation point gets contributions from both parts of the field, leading to the double strength in [\(5.3b\)](#).

In the special case $\kappa_- = \kappa_+$, the leading term in [\(5.3\)](#) vanishes. In this case, the error terms in [\(5.3\)](#) can be tightened, as shown in [Appendixes A, B, and C](#), with the outcome that the transition rate remains bounded on approaching the horizon.

In the Unruh state, we find

$$\dot{\mathcal{F}}_U^L(\omega, \tau, \tau_0) = \frac{1}{4\pi(\tau_h - \tau)} \left(\frac{\kappa_+}{\kappa_-} - 1 + o(1) \right), \quad (5.4a)$$

$$\dot{\mathcal{F}}_U^R(\omega, \tau, \tau_0) = -\frac{1 + o(1)}{4\pi(\tau_h - \tau)}, \quad (5.4b)$$

$$\dot{\mathcal{F}}_U^0(\omega, \tau, \tau_0) = \frac{1}{4\pi(\tau_h - \tau)} \left(\frac{\kappa_+}{\kappa_-} - 2 + o(1) \right). \quad (5.4c)$$

The divergence on approaching H_-^L is as in the HHI state, but the divergence on approaching H_-^R is independent of the surface gravities, and has always a negative sign. The divergence on approaching the bifurcation point is the sum.

In the special case $\kappa_- = \kappa_+$, the leading term in [\(5.4a\)](#) vanishes, and we show in [Appendix A](#) that $\dot{\mathcal{F}}_U^L$ remains bounded on approaching H_-^L . In the special case $\kappa_+ = 2\kappa_-$, the leading term in [\(5.4c\)](#) vanishes, and we show in [Appendixes B and C](#) that

$$\dot{\mathcal{F}}_U^0(\omega, \tau, \tau_0) = \frac{1 + o(1)}{2\pi(\tau_h - \tau)(-\ln(\tau_h - \tau))}, \quad (5.5)$$

which diverges on approaching the bifurcation point, but less quickly than $1/(\tau_h - \tau)$.

VI. ENERGY NEAR THE CAUCHY HORIZON

In this section, we compare the transition rate results of [Sec. V](#) to the energy density seen by a geodesic observer.

A. HHI state

Recall from [\(2.8\)](#) that in the Kruskal coordinates (U, V) , we have

$$ds^2 = \Omega_K^2(-dU dV), \quad (6.1)$$

where

$$\Omega_K^2 = -\frac{F}{\kappa_+^2 UV}, \quad (6.2)$$

and r is determined as a function of r by [\(2.9\)](#) for $UV < 0$ and by [\(2.10\)](#) for $UV > 0$. As the HHI state is built on the positive frequency definition provided by ∂_U and ∂_V , conformal invariance of the field shows that the renormalized stress-energy tensor T_{ab}^{HHI} in the HHI state is given by^{30,61,62}

$$T_{ab}^{\text{HHI}}(x) = \Xi_{ab}(x) - \frac{R(x)}{48\pi} g_{ab}, \quad (6.3)$$

where

$$\Xi_{UU} = -(1/12\pi)\Omega_K\partial_U^2\Omega_K^{-1}, \quad (6.4a)$$

$$\Xi_{VV} = -(1/12\pi)\Omega_K\partial_V^2\Omega_K^{-1}, \quad (6.4b)$$

$$\Xi_{UV} = \Xi_{VU} = 0, \quad (6.4c)$$

and R is the Ricci scalar.

The energy density on a timelike worldline parametrized by the proper time τ is given by

$$\begin{aligned} \mathcal{E}_H &= \dot{x}^a \dot{x}^b T_{ab}^{\text{HHI}} \\ &= \dot{U}^2 \Xi_{UU} + \dot{V}^2 \Xi_{VV} + \frac{R}{48\pi} \\ &= -\frac{(\dot{u}^2 + \dot{v}^2)}{192\pi} (F'^2 - 2FF'' - 4\kappa_+^2) + \frac{R}{48\pi}, \end{aligned} \quad (6.5)$$

where the overdots denote derivative with respect to τ , and the last expression, using the coordinates (\tilde{u}, \tilde{v}) , assumes the worldline to be in region II. Near the Cauchy horizon, we have

$$F'^2 - 2FF'' = 4\kappa_-^2 + \mathcal{O}((r - r_-)^2), \quad (6.6)$$

and the Ricci scalar remains bounded. For a geodesic approaching the Cauchy horizon, it then follows from the estimates given for $\tilde{u}(\tau)$, $\tilde{v}(\tau)$, and $r(\tau)$ in [Appendixes A, B, and C](#) that

$$\begin{aligned} \mathcal{E}_H^L(\tau) &= \mathcal{E}_H^R(\tau) \\ &= \frac{(1 + \mathcal{O}(\tau_h - \tau))}{48\pi(\tau_h - \tau)^2} \left(\frac{\kappa_+^2}{\kappa_-^2} - 1 \right) + \mathcal{O}(1), \end{aligned} \quad (6.7a)$$

$$\mathcal{E}_H^0(\tau) = \frac{1}{24\pi(\tau_h - \tau)^2} \left(\frac{\kappa_+^2}{\kappa_-^2} - 1 \right) + \mathcal{O}(1), \quad (6.7b)$$

where the superscripts L , R , and 0 indicate whether the geodesic approaches the Cauchy horizon at H_-^L , H_-^R , or the bifurcation point. Note that when $\kappa_+ = \kappa_-$, the energy density remains bounded in all three cases.

B. Unruh state

We proceed similarly with the Unruh state. In the hybrid coordinates (U, v) , the metric [\(2.12\)](#) reads

$$ds^2 = \Omega_U^2(-dU dv), \quad (6.8)$$

where

$$\Omega_U^2 = -\frac{F}{\kappa_+ U}, \quad (6.9)$$

and r is determined as a function of U and v from [\(2.13\)](#). The renormalized stress-energy tensor T_{ab}^{Unruh} in the Unruh state is given by

$$T_{ab}^U(x) = \Psi_{ab}(x) - \frac{R(x)}{48\pi} g_{ab}, \quad (6.10)$$

where

$$\Psi_{UU} = -(1/12\pi)\Omega_U \partial_U^2 \Omega_U^{-1}, \quad (6.11a)$$

$$\Psi_{vv} = -(1/12\pi)\Omega_U \partial_v^2 \Omega_U^{-1}, \quad (6.11b)$$

$$\Psi_{Uv} = \Psi_{vU} = 0. \quad (6.11c)$$

The energy density on a timelike worldline parametrized by the proper time τ is now given by

$$\begin{aligned} \mathcal{E}_U &= \dot{x}^a \dot{x}^b T_{ab}^U \\ &= \dot{U}^2 \Psi_{UU} + \dot{v}^2 \Psi_{vv} + \frac{R}{48\pi} \\ &= -\frac{\dot{u}^2}{192\pi} (F'^2 - 2FF'' - 4\kappa_+^2) - \frac{\dot{v}^2}{192\pi} (F'^2 - 2FF'') + \frac{R}{48\pi}, \end{aligned} \quad (6.12)$$

where the last expression assumes the worldline to be in region II. For a geodesic approaching the Cauchy horizon, proceeding as with (6.7) and using the same notation, we find

$$\mathcal{E}_U^L(\tau) = \frac{(1 + \mathcal{O}(\tau_h - \tau))}{48\pi(\tau_h - \tau)^2} \left(\frac{\kappa_+^2}{\kappa_-^2} - 1 \right) + \mathcal{O}(1), \quad (6.13a)$$

$$\mathcal{E}_U^R(\tau) = -\frac{1 + \mathcal{O}(\tau_h - \tau)}{48\pi(\tau_h - \tau)^2}, \quad (6.13b)$$

$$\mathcal{E}_U^0(\tau) = \frac{1}{48\pi(\tau_h - \tau)^2} \left(\frac{\kappa_+^2}{\kappa_-^2} - 2 \right) + \mathcal{O}(1). \quad (6.13c)$$

Note that \mathcal{E}_U^L remains bounded when $\kappa_+ = \kappa_-$, \mathcal{E}_U^0 remains bounded when $\kappa_+ = \sqrt{2}\kappa_-$, and \mathcal{E}_U^R diverges for all values of κ_+ and κ_- .

C. Comparison

Comparing (5.3) with (6.7), and (5.4) with (6.13), we see that there is a significant qualitative and quantitative agreement between the divergence of the detector's transition rate and the divergence of the observer's energy density on approaching the Cauchy horizon.

For both the HHI and Unruh states, neither quantity diverges on H_-^L when $\kappa_+ = \kappa_-$, whereas both quantities diverge for $\kappa_+ \neq \kappa_-$, and the sign of the divergence agrees, being positive for $\kappa_- < \kappa_+$ and negative for $\kappa_+ < \kappa_-$. On H_-^R , the situation for the HHI state is similar, whereas for the Unruh state there is always a divergence with a negative overall coefficient. The Cauchy horizon bifurcation point interpolates between the two branches; in the Unruh state, the threshold between positive and negative divergence occurs at $\kappa_+ = 2\kappa_-$ with the transition rate and at $\kappa_+ = \sqrt{2}\kappa_-$ with the energy density.

When a divergence occurs, it is proportional to $(\tau_h - \tau)^{-1}$ in the transition rate and proportional to $(\tau_h - \tau)^{-2}$ in the energy density. In the integral of the energy density over a finite proper time interval, the divergence is proportional to $(\tau_h - \tau)^{-1}$.

VII. THE RINDLER HORIZON

In this section, we consider the transition rate and the energy density in the closely analogous situation of an inertial observer approaching the Rindler horizon in (1 + 1)-dimensional Minkowski

spacetime, coupled to a massless scalar field in its Rindler state. We also contrast this situation with known results in (3 + 1)-dimensional Minkowski spacetime.

A. 1 + 1 Rindler

We consider (1 + 1)-dimensional Minkowski spacetime with the metric

$$ds^2 = -dt^2 + dx^2, \quad (7.1)$$

and therein the right-hand-side Rindler wedge, $|t| < x$, and therein the geodesic

$$(t, x) = (\tau, \tau_h), \quad (7.2)$$

parametrized by the proper time τ , where τ_h is a positive constant, and the range of τ within the Rindler wedge is $-\tau_h < \tau < \tau_h$. As $\tau \rightarrow \tau_h$, the trajectory approaches the future Rindler horizon.

We take the scalar field to be in the Rindler state, for which the positive frequencies are defined with respect to the boost Killing vector $x\partial_t + t\partial_x$. The Wightman function reads⁶²

$$\mathcal{W}_R(x, x') = -\frac{1}{4\pi} \ln [(\epsilon + i\Delta u)(\epsilon + i\Delta v)], \quad (7.3)$$

where the coordinates (u, v) are defined by $u = -\ln(a(x - t))$ and $v = \ln(a(x + t))$; $\Delta u = u - u'$ and $\Delta v = v - v'$; the ϵ -notation specifies the branches of the logarithm as in Sec. III; and a is a positive constant of dimension inverse length that we have included for dimensional consistency. In the coordinates (u, v) , the geodesic (7.2) reads

$$u(\tau) = -\ln(a(\tau_h - \tau)), \quad (7.4a)$$

$$v(\tau) = \ln(a(\tau_h + \tau)). \quad (7.4b)$$

Following the notation of Sec. V, we denote the detector's switch-on moment by τ_0 and switch-off moment by τ , where $-\tau_h < \tau_0 < \tau < \tau_h$, and we consider the asymptotic behavior of the transition rate $\dot{\mathcal{F}}(\omega, \tau, \tau_0)$ (4.2) as $\tau \rightarrow \tau_h$, with τ_0 fixed.

Proceeding as in Sec. V, we find that the Δv -dependent part of \mathcal{W}_R (7.3) remains bounded as $\tau \rightarrow \tau_h$, whereas, by comparison of (7.4a) and (B2), the contributions from the Δu -dependent part obey the same estimates that were found in Appendix B for approaching H_-^R in the Unruh state. We find

$$\dot{\mathcal{F}}_R(\omega, \tau, \tau_0) = -\frac{1}{4\pi(\tau_h - \tau)} + \frac{1 + o(1)}{2\pi(\tau_h - \tau)(-\ln(\tau_h - \tau))}, \quad (7.5)$$

where the subscript R refers to the Rindler state.

The renormalized stress-energy tensor T_{ab}^R in the Rindler state can be evaluated by the conformal scaling technique as in (6.3) and (6.10), and is well known.⁶³ The energy density seen by an observer on the trajectory (7.2) evaluates to

$$\begin{aligned} \mathcal{E}_R &= \dot{x}^a \dot{x}^b T_{ab}^R \\ &= -\frac{1}{48\pi} \left(\frac{1}{(\tau_h - \tau)^2} + \frac{1}{(\tau_h + \tau)^2} \right). \end{aligned} \quad (7.6)$$

We see that the divergences in the transition rate (7.5) and the energy density (7.6) are similar to those on approaching the H_-^R branch of the Cauchy horizon in the black hole spacetime when the

field is in the Unruh state, found in Secs. V and VI, including the sign of the divergence and the power law of the divergence.

B. 3 + 1 Rindler

In 3 + 1 spacetime dimensions, an inertial detector approaching the Rindler horizon was analyzed in Ref. 26, taking the field to be in the Rindler state and assuming that the detector’s coupling to the field does not include a derivative. In our notation of (7.2), the result for the transition rate reads

$$\dot{\mathcal{F}}_{R,3+1}(\omega, \tau, \tau_0) = \frac{1}{8\pi^2\tau_h} \left\{ \ln \left(1 - \frac{\tau}{\tau_h} \right) + 2 \ln \left[-\ln \left(1 - \frac{\tau}{\tau_h} \right) + \mathcal{O}(1) \right] \right\}. \quad (7.7)$$

The energy density seen by this inertial observer can be found using the Rindler state stress-energy tensor given in Ref. 63, with the result

$$\begin{aligned} \mathcal{E}_{R,3+1} &= \dot{x}^a \dot{x}^b T_{ab}^{R,3+1} \\ &= -\frac{3\tau_h^2 + \tau^2}{1440\pi^2(\tau_h^2 - \tau^2)^3}. \end{aligned} \quad (7.8)$$

C. Comparison of 1 + 1 and 3 + 1

One might have expected an agreement in the leading divergences of the transition rate $\dot{\mathcal{F}}_R$ (7.5) and $\dot{\mathcal{F}}_{R,3+1}$ (7.7), given the differing short-separation divergences of the Wightman function in 1 + 1 and 3 + 1 dimensions,²⁹ and the inclusion of time derivative in the coupling in 1 + 1 dimensions but not in 3 + 1 dimensions. Yet the divergences do not agree: Instead, the leading divergences of $\dot{\mathcal{F}}_R$ agree with the divergences of the τ -derivative of $\dot{\mathcal{F}}_{R,3+1}$.

These properties of the Rindler state suggest the conjecture that in 3 + 1 spacetime dimensions, a detector coupled linearly to the value (as opposed to the derivative) of the scalar field, and approaching a Cauchy horizon, may have a transition rate that diverges only logarithmically in proper time. We leave the investigation of this conjecture to future work.

VIII. CONCLUSIONS

We have investigated the internal transitions in a space-and-time localized quantum system on geodesics that approach the Cauchy horizon in a (1 + 1)-dimensional eternal black hole spacetime whose global structure mimics that of the non-extremal Reissner–Nordström solution. The quantum system was a spatially pointlike Unruh–DeWitt detector, coupled linearly to the proper time derivative of a massless scalar field, which was prepared initially in the HHI state or the Unruh state. Working in first-order perturbation theory, we found that the detector’s transition rate generically diverges on approaching the Cauchy horizon, proportionally to the inverse proper time to the horizon. The exception was when the surface gravities of the two horizons are equal: In this case, the transition rate remains bounded on all parts of the Cauchy horizon in the HHI state, and on one branch of the Cauchy horizon in the Unruh state. We also saw that these properties of the detector’s transition rate have a close

qualitative and quantitative similarity with the energy density seen by an observer falling toward the Cauchy horizon. Finally, by comparison with results for the Rindler state and Rindler horizon, we conjectured that a similar but weaker divergence may be present in 3 + 1 spacetime dimensions in the transition rate of a detector coupled linearly to the value (rather than to the proper time derivative) of the quantum field.

That horizons with equal surface gravities emerge as the exceptionally regular special case may not be surprising: That this case is special was already known from consideration of the stress-energy tensor,^{15–17} and similar observations arise with “lukewarm” black holes, in which two Killing horizons bound a spacetime region in which the Killing vector in question is timelike.^{64,65} It is however notable that in the HHI state, the overall sign of the leading divergence is determined by which of the two surface gravities is greater, in precisely the same way for both the detector’s transition rate and for the energy density seen by an observer. In comparison, for a detector falling to the singularity of the (1 + 1)-dimensional Schwarzschild spacetime, the leading divergence in the detector’s transition rate has always a positive sign, both in the HHI state and in the Unruh state.²⁷ This highlights the differences between a Cauchy horizon and a Schwarzschild-type singularity.

We emphasize that a negative transition rate is not as such physically pathological, given the operational definition of the transition rate in terms of ensembles of detectors, switched off at different times.^{26,34} That the integral of the transition rate can diverge to negative infinity may be more disconcerting, but this is just an artifact of our passing to the sharp switching limit, and dropping the concomitant infinite additive constant from the transition probability. If the sharp switching is replaced by a smooth switching, all probabilities are by construction non-negative, but disentangling the switching effects from the spacetime effects becomes less transparent, as exemplified by a smoothly switched detector that falls in the (3 + 1)-dimensional Schwarzschild black hole.⁶⁶

Our techniques can be extended to more general spacetimes with horizons, such as degenerate horizons,⁶⁷ or to spacetimes in which spacetime singularities have been resolved by nonlinear effects⁶⁸ or by quantum gravity effects.⁶⁹ We leave such extensions subject to future work.

ACKNOWLEDGMENTS

We thank Bernard Kay, Adrian Ottewill, and Silke Weinfurter for helpful discussions and comments. B.A.J.-A. is supported by a CONACYT Postdoctoral Research Fellowship, and acknowledges in addition the support of CONACYT Project No. 140630 and UNAM-DGAPA-PAPIIT Grant No. IG100120. J.L. was supported in part by United Kingdom Research and Innovation (UKRI) Science and Technology Facilities Council (STFC) Grant No. ST/S002227/1 “Quantum Sensors for Fundamental Physics” and Theory Consolidated Grant No. ST/P000703/1.

AUTHOR DECLARATIONS

Conflict of Interest

The authors have no conflicts to disclose.

DATA AVAILABILITY

Data sharing is not applicable to this article as no new data were created or analyzed in this study.

APPENDIX A: $\dot{\mathcal{F}}$ NEAR H_-^L

In this appendix, we perform the estimates that lead from (5.2) to the results stated in Sec. V for the asymptotics of $\dot{\mathcal{F}}$ near H_-^L .

1. Preliminaries

Recall that the geodesic is by assumption in region II, where $(U, V) \in \mathbb{R}_+ \times \mathbb{R}_+$ and $(\tilde{u}, \tilde{v}) \in \mathbb{R} \times \mathbb{R}$. The geodesic is an integral curve of the system (2.18), or equivalently (2.19). Differentiating (2.19) gives

$$\ddot{\tilde{u}} = -\frac{1}{2}\dot{\tilde{u}}^2 F'(r), \tag{A1a}$$

$$\ddot{\tilde{v}} = -\frac{1}{2}\dot{\tilde{v}}^2 F'(r), \tag{A1b}$$

which will be useful below.

From (3.3) and (3.5) we have, for $\tau' < \tau$,

$$\mathcal{W}_H(\tau, \tau') = -\frac{1}{4\pi} \ln [U(\tau) - U(\tau')] - \frac{1}{4\pi} \ln [V(\tau) - V(\tau')] - \frac{i}{4}, \tag{A2a}$$

$$\mathcal{W}_U(\tau, \tau') = -\frac{1}{4\pi} \ln [U(\tau) - U(\tau')] - \frac{1}{4\pi} \ln [v(\tau) - v(\tau')] - \frac{i}{4}, \tag{A2b}$$

and hence

$$\partial_\tau \mathcal{W}_H(\tau, \tau') = -\frac{\kappa_+}{4\pi} \times \frac{\dot{\tilde{u}}(\tau)}{1 - U(\tau')/U(\tau)} - \frac{\kappa_+}{4\pi} \times \frac{\dot{\tilde{v}}(\tau)}{1 - V(\tau')/V(\tau)}, \tag{A3a}$$

$$\partial_\tau \mathcal{W}_U(\tau, \tau') = -\frac{\kappa_+}{4\pi} \times \frac{\dot{\tilde{u}}(\tau)}{1 - U(\tau')/U(\tau)} - \frac{1}{4\pi} \times \frac{\dot{\tilde{v}}(\tau)}{\tilde{v}(\tau) - \tilde{v}(\tau')}. \tag{A3b}$$

Expanding (A3) in $\tau - \tau'$, using (2.19) and (A1), we find

$$\lim_{\tau' \rightarrow \tau} \left(\partial_\tau \mathcal{W}_H(\tau, \tau') + \frac{1}{2\pi(\tau - \tau')} \right) = \frac{[\dot{\tilde{u}}(\tau) + \dot{\tilde{v}}(\tau)] [F'(r(\tau)) - 2\kappa_+]}{16\pi}, \tag{A4a}$$

$$\lim_{\tau' \rightarrow \tau} \left(\partial_\tau \mathcal{W}_U(\tau, \tau') + \frac{1}{2\pi(\tau - \tau')} \right) = \frac{\dot{\tilde{u}}(\tau) [F'(r(\tau)) - 2\kappa_+] + \dot{\tilde{v}}(\tau) F'(r(\tau))}{16\pi}. \tag{A4b}$$

2. Geodesics approaching H_-^L

We now specialize to the geodesics approaching H_-^L , which are those with $E > 0$. It follows from (2.18b) that $r(\tau) \rightarrow r_-$ smoothly and with a nonvanishing derivative as $\tau \rightarrow \tau_h$. As $\tau \rightarrow \tau_h$, \tilde{v} increases smoothly to a finite value and V increases smoothly to a finite positive value, whereas $\tilde{u} \rightarrow \infty$, logarithmically in $\tau_h - \tau$, and $U \rightarrow \infty$, as an inverse power law in $\tau_h - \tau$.

Given the above observations, and setting $\tau' = \tau_0$ in (A3), we see that the only contributions to $\dot{\mathcal{F}}(\omega, \tau, \tau_0)$ in (5.2) that may be potentially unbounded as $\tau \rightarrow \tau_h$ come from those terms in (A3) and (A4) that involve $\dot{\tilde{u}}$, and these terms are the same for the HHI and Unruh states. We may hence drop the reference to the state.

3. First boundary term in (5.2)

Let $B_1(\tau, \tau_0, \omega)$ denote the first term on the right-hand side of (5.2),

$$B_1(\tau, \tau_0, \omega) \doteq -2 \cos(\omega \Delta \tau) \partial_\tau \mathcal{W}(\tau, \tau_0). \tag{A5}$$

For $\mathcal{W}(\tau, \tau_0)$, (A3) with $\tau' = \tau_0$ gives

$$\partial_\tau \mathcal{W}(\tau, \tau_0) = -\frac{\kappa_+ \dot{\tilde{u}}(\tau)}{4\pi} \left[1 + \mathcal{O}\left(\frac{U(\tau_0)}{U(\tau)}\right) \right] + \mathcal{O}(1). \tag{A6}$$

To estimate $\dot{\tilde{u}}$, we write

$$F(r) = -2\kappa_-(r - r_-) + \mathcal{O}((r - r_-)^2), \tag{A7}$$

by which (2.19a) gives

$$\dot{\tilde{u}} = \frac{E}{\kappa_-(r - r_-)} + \mathcal{O}(1), \tag{A8}$$

and (2.18b) gives

$$r - r_- = E(\tau_h - \tau) + \mathcal{O}((\tau_h - \tau)^2), \tag{A9}$$

whence

$$\dot{\tilde{u}}(\tau) = \frac{1}{\kappa_-(\tau_h - \tau)} + \mathcal{O}(1). \tag{A10}$$

For $U(\tau_0)/U(\tau)$, we have

$$\begin{aligned} \frac{U(\tau_0)}{U(\tau)} &= \exp[\kappa_+(\tilde{u}(\tau_0) - \tilde{u}(\tau))] \\ &= \exp\left[-\kappa_+ \int_{\tau_0}^{\tau} dt' \dot{\tilde{u}}(t')\right] \\ &= \exp\left[-\frac{\kappa_+}{\kappa_-} \int_{\tau_0}^{\tau} dt' \left(\frac{1}{\tau_h - t'} + \mathcal{O}(1)\right)\right] \\ &= \exp\left[\frac{\kappa_+}{\kappa_-} \ln\left(\frac{\tau_h - \tau}{\tau_h - \tau_0}\right) + \mathcal{O}(1)\right] \\ &= \left(\frac{\tau_h - \tau}{\tau_h - \tau_0}\right)^{\kappa_+/\kappa_-} \times e^{\mathcal{O}(1)} \\ &= \mathcal{O}((\tau_h - \tau)^{\kappa_+/\kappa_-}). \end{aligned} \tag{A11}$$

Collecting, we have

$$B_1(\tau, \tau_0, \omega) = \frac{\cos(\omega \Delta \tau)}{2\pi(\tau_h - \tau)} \left(\frac{\kappa_+}{\kappa_-} + \mathcal{O}(\tau_h - \tau) + \mathcal{O}((\tau_h - \tau)^{\kappa_+/\kappa_-}) \right). \tag{A12}$$

4. Second boundary term in (5.2)

Let $B_2(\tau, \tau_0, \omega)$ denote the second term on the right-hand side of (5.2). From (A4), we have

$$B_2(\tau, \tau_0, \omega) = \frac{\dot{\tilde{u}}(\tau) [F'(r(\tau)) - 2\kappa_+]}{8\pi} + \mathcal{O}(1). \tag{A13}$$

Using (A7), (A9), and (A10), we obtain

$$B_2(\tau, \tau_0, \omega) = -\frac{1}{4\pi(\tau_h - \tau)} \left(\frac{\kappa_+}{\kappa_-} + 1 \right) + \mathcal{O}(1). \tag{A14}$$

5. Integral term in (5.2)

Let $J(\tau, \tau_0, \omega)$ denote the integral term on the right-hand side of (5.2). As the contribution from the term $(\tau - \tau')^{-1} \sin(\omega(\tau - \tau'))$ in the integrand is $\mathcal{O}(1)$, using (A3) gives

$$J(\omega, \tau, \tau_0) = \frac{\kappa_+ \omega}{2\pi} \dot{u}(\tau) I(\omega, \tau, \tau_0) + \mathcal{O}(1), \tag{A15}$$

where

$$I(\omega, \tau, \tau_0) \doteq \int_{\tau_0}^{\tau} d\tau' \frac{\sin(\omega(\tau - \tau'))}{1 - U(\tau')/U(\tau)}. \tag{A16}$$

We shall show that the leading contribution in $I(\omega, \tau, \tau_0)$ is $\mathcal{O}(1)$ and evaluate this contribution.

Changing variables in (A16) by $\tau' = \tau - s$ gives

$$I(\omega, \tau, \tau_0) = I_1(\omega, \tau, \tau_0) + I_2(\omega, \tau, \tau_0), \tag{A17a}$$

$$I_1(\omega, \tau, \tau_0) = \int_0^{\tau_h - \tau_0} ds \frac{\sin(\omega s)}{1 - U(\tau - s)/U(\tau)}, \tag{A17b}$$

$$I_2(\omega, \tau, \tau_0) = - \int_{\tau - \tau_0}^{\tau_h - \tau_0} ds \frac{\sin(\omega s)}{1 - U(\tau - s)/U(\tau)}, \tag{A17c}$$

where in I_1 (A17b), the upper limit of integration has been extended from $\tau - \tau_0$ to $\tau_h - \tau_0$, and I_2 (A17c) has been introduced to compensate for this. The extension is well defined provided $\tau_h - \tau$ is so small that the detector's trajectory may be extended from proper time τ_0 backward to proper time $\tau_0 - (\tau_h - \tau)$, still in region II, which we may assume without loss of generality.

For I_2 (A17c), we have

$$\begin{aligned} |I_2| &\leq \int_{\tau - \tau_0}^{\tau_h - \tau_0} \frac{ds}{1 - U(\tau - s)/U(\tau)} \\ &\leq \int_{\tau - \tau_0}^{\tau_h - \tau_0} \frac{ds}{1 - U(\tau_0)/U(\tau)} \\ &= \frac{\tau_h - \tau}{1 - U(\tau_0)/U(\tau)} = \mathcal{O}(\tau_h - \tau), \end{aligned} \tag{A18}$$

using that U is a positive and increasing function of its argument.

For I_1 (A17b), we shall show below in Subsection 7 of Appendix A that

$$\begin{aligned} I_1(\omega, \tau, \tau_0) &= \frac{1 - \cos(\omega(\tau_h - \tau_0))}{\omega} + o(1) \\ &= \frac{1 - \cos(\omega\Delta\tau)}{\omega} + o(1), \end{aligned} \tag{A19}$$

where in the second equality τ_h has been replaced by τ at the expense of an $\mathcal{O}(\tau_h - \tau)$ error, covered by the $o(1)$ term.

Collecting, and using (A10), we have

$$J(\omega, \tau, \tau_0) = \frac{(\kappa_+/\kappa_-)}{2\pi(\tau_h - \tau)} [1 - \cos(\omega\Delta\tau) + o(1)]. \tag{A20}$$

6. Combining

Adding (A12), (A14), and (A20) gives

$$\frac{1}{4\pi(\tau_h - \tau)} \left(\frac{\kappa_+}{\kappa_-} - 1 + o(1) \right), \tag{A21}$$

which is the result shown in (5.3a) and (5.4a).

7. Interlude: Estimate for I_1 (A17b)

We now establish the estimate (A19) for I_1 (A17b).

Recall that U is a positive and strictly increasing function of the proper time along the geodesic, with the asymptotics (A11) near the Cauchy horizon. It follows that we can write

$$I_1(\omega, \tau, \tau_0) = K(\tau_h - \tau, \tau_h - \tau_0), \tag{A22}$$

where

$$K(\epsilon, m, \omega) \doteq \int_0^m ds \frac{\sin(\omega s)}{1 - \frac{H(\epsilon + s)}{H(\epsilon)}}, \tag{A23}$$

such that $H(x) = x^{-A} \tilde{H}(x)$, $A = \kappa_+/\kappa_-$ is a positive constant, \tilde{H} is a smooth positive function on $[0, R]$ for some $R > 0$, $H' < 0$ on $(0, R]$, $0 < m < R$ and $0 < \epsilon < R - m$. We consider m and ω as parameters and wish to find $\lim_{\epsilon \rightarrow 0} K(\epsilon, m, \omega)$.

For fixed positive s , the ratio $H(\epsilon + s)/H(\epsilon)$ in (A23) tends to zero as $\epsilon \rightarrow 0$. If the limit $\epsilon \rightarrow 0$ can be taken under the integral, we hence have

$$\begin{aligned} \lim_{\epsilon \rightarrow 0} K(\epsilon, m, \omega) &= \int_0^m ds \sin(\omega s) \\ &= \frac{1 - \cos(\omega m)}{\omega}, \end{aligned} \tag{A24}$$

from which the first equality in (A19) follows. We shall show that taking the limit under the integral is justified by dominated convergence.

From $H(x) = x^{-A} \tilde{H}(x)$ and the properties of \tilde{H} , it follows that there exists $\epsilon_1 \in (0, R/2)$ such that $\partial_x^2 \ln(H(x)) > 0$ for $0 < x < 2\epsilon_1$. This implies that we have

$$\frac{\partial}{\partial \epsilon} \left[1 - \frac{H(\epsilon + s)}{H(\epsilon)} \right] = \frac{H(\epsilon + s)}{H(\epsilon)} \left[\frac{H'(\epsilon)}{H(\epsilon)} - \frac{H'(\epsilon + s)}{H(\epsilon + s)} \right] < 0, \tag{A25}$$

for $s \in (0, \epsilon_1]$ and $\epsilon \in (0, \epsilon_1)$.

Taking from now on $\epsilon \in (0, \epsilon_1)$, we split (A23) as

$$K(\epsilon, m, \omega) = K_{<}(\epsilon, m, \omega) + K_{>}(\epsilon, m, \omega), \tag{A26a}$$

$$K_{<}(\epsilon, m, \omega) = \int_0^{\epsilon_1} ds \frac{\sin(\omega s)}{1 - \frac{H(\epsilon + s)}{H(\epsilon)}}, \tag{A26b}$$

$$K_{>}(\epsilon, m, \omega) = \int_{\epsilon_1}^m ds \frac{\sin(\omega s)}{1 - \frac{H(\epsilon + s)}{H(\epsilon)}}. \tag{A26c}$$

By (A25), the integrand in (A26b) is bounded in absolute value by

$$\left| \frac{\sin(\omega s)}{1 - \frac{H(\epsilon + s)}{H(\epsilon)}} \right| \leq \frac{|\sin(\omega s)|}{1 - \frac{H(\epsilon_1 + s)}{H(\epsilon_1)}}, \tag{A27}$$

which is independent of ϵ and integrable over $s \in (0, \epsilon_1)$. The integrand in (A26c) is bounded in absolute value by

$$\left| \frac{\sin(\omega s)}{1 - \frac{H(\epsilon + s)}{H(\epsilon)}} \right| \leq \frac{1}{1 - \frac{H(\epsilon + \epsilon_1)}{H(\epsilon)}} \leq \frac{1}{1 - \frac{H(2\epsilon_1)}{H(\epsilon_1)}}, \tag{A28}$$

where the first equality comes because H is decreasing and the last inequality comes by (A25). The last expression in (A28) is independent of ϵ and integrable over $s \in (\epsilon_1, m)$. This completes the dominated convergence argument.

8. Special case $\kappa_+ = \kappa_-$

We now consider the special case $\kappa_+ = \kappa_-$, in which the leading term in (A21) vanishes. We show that the transition rate remains bounded as $\tau \rightarrow \tau_h$.

The contributions from the parts involving \dot{v} in (A3) and (A4) remain bounded as $\tau \rightarrow \tau_h$. The \mathcal{O} -terms in $B_1(\tau, \tau_0, \omega)$ (A12) now combine to $\mathcal{O}(\tau_h - \tau)$. What needs a better estimate is $I_1(\omega, \tau, \tau_0)$, given by (A22) and (A23), now with $A = 1$.

In (A23), setting $A = 1$ and isolating the leading behavior gives

$$K(\epsilon, m, \omega) = K_0(m, \omega) + \epsilon K_1(\epsilon, m, \omega), \tag{A29a}$$

$$K_0(m, \omega) = \int_0^m ds \sin(\omega s) = \frac{1 - \cos(\omega m)}{\omega}, \tag{A29b}$$

$$K_1(\epsilon, m, \omega) = \frac{1}{\tilde{H}(\epsilon)} \int_0^m ds \frac{\sin(\omega s)}{s} \times \frac{s}{g(\epsilon + s) - g(\epsilon)}, \tag{A29c}$$

where $g(x) \doteq x/\tilde{H}(x)$ for $x > 0$ and $g(0) \doteq 0$. As g is smooth and satisfies $g'(x) > 0$ for $x \in [0, R]$, there exists a positive constant k_1 , independent of ϵ , such that $k_1 s \leq g(\epsilon + s) - g(\epsilon)$ for $s \in [0, m]$ and sufficiently small ϵ . Dominated convergence hence implies

$$\lim_{\epsilon \rightarrow 0} K_1(\epsilon, m, \omega) = \frac{1}{\tilde{H}(0)} \int_0^m ds \frac{\sin(\omega s)}{s} \tilde{H}(s), \tag{A30}$$

which is finite.

Combining, it follows that $\dot{\mathcal{F}}(\omega, \tau, \tau_0)$ remains bounded as $\tau \rightarrow \tau_0$.

APPENDIX B: $\dot{\mathcal{F}}$ NEAR H_-^R

In this appendix, we perform the estimates that lead from (5.2) to the results stated in Sec. V for the asymptotics of $\dot{\mathcal{F}}$ near H_-^R .

The geodesics in question are those with $E < 0$ in (2.18) and (2.19).

As the HHI state is invariant under right-left reflection, $(U, V) \mapsto (V, U)$, the result for the HHI state is the same whether the Cauchy horizon branch is H_-^p or H_-^E . This gives the result shown in (5.3a).

For the Unruh state, the contributions from the parts in (A3b) and (A4b) that involve \dot{u} are smooth as $\tau \rightarrow \tau_0$. We need to consider the contributions from the parts that involve \dot{v} .

1. First boundary term in (5.2)

Consider the first term on the right-hand side of (5.2), given by $B_1(\tau, \tau_0, \omega)$ (A5). For $\mathcal{W}(\tau, \tau_0)$, (A3b) with $\tau' = \tau_0$ gives

$$\partial_\tau \mathcal{W}_U(\tau, \tau_0) = -\frac{1}{4\pi} \times \frac{\dot{v}(\tau)}{\tilde{v}(\tau) - \tilde{v}(\tau_0)} + \mathcal{O}(1). \tag{B1}$$

Proceeding as with (A10) gives

$$\dot{v}(\tau) = \frac{1}{\kappa_-(\tau_h - \tau)} + \mathcal{O}(1). \tag{B2}$$

Hence

$$B_1(\tau, \tau_0, \omega) = \frac{\cos(\omega\Delta\tau)}{2\pi(\tau_h - \tau)(-\ln(\tau_h - \tau) + \mathcal{O}(1))}. \tag{B3}$$

2. Second boundary term in (5.2)

For the second term on the right-hand side of (5.2), $B_2(\tau, \tau_0, \omega)$, (A4b) gives

$$B_2(\tau, \tau_0, \omega) = \frac{\dot{v}(\tau)F'(r(\tau))}{16\pi} + \mathcal{O}(1). \tag{B4}$$

Proceeding as with (A14) gives

$$B_2(\tau, \tau_0, \omega) = -\frac{1}{4\pi(\tau_h - \tau)} + \mathcal{O}(1). \tag{B5}$$

3. Integral term in (5.2)

Let $J(\tau, \tau_0, \omega)$ again denote the integral term on the right-hand side of (5.2). Proceeding as with (A15), using (A3b) gives

$$J(\omega, \tau, \tau_0) = \frac{\omega\dot{v}(\tau)}{2\pi\tilde{v}(\tau)} \tilde{I}(\omega, \tau, \tau_0) + \mathcal{O}(1), \tag{B6}$$

where

$$\tilde{I}(\omega, \tau, \tau_0) \doteq \int_{\tau_0}^\tau dt' \frac{\sin(\omega(\tau - t'))}{1 - \tilde{v}(t')/\tilde{v}(\tau)}, \tag{B7}$$

and we are assuming τ to be so close to τ_h that $\tilde{v}(\tau)$ is positive. Proceeding as in (A17), we have

$$\tilde{I}(\omega, \tau, \tau_0) = \tilde{I}_1(\omega, \tau, \tau_0) + \tilde{I}_2(\omega, \tau, \tau_0), \tag{B8a}$$

$$\tilde{I}_1(\omega, \tau, \tau_0) = \int_0^{\tau_h - \tau_0} ds \frac{\sin(\omega s)}{1 - \tilde{v}(\tau - s)/\tilde{v}(\tau)}, \tag{B8b}$$

$$\tilde{I}_2(\omega, \tau, \tau_0) = -\int_{\tau - \tau_0}^{\tau_h - \tau_0} ds \frac{\sin(\omega s)}{1 - \tilde{v}(\tau - s)/\tilde{v}(\tau)}. \tag{B8c}$$

For \tilde{I}_2 (B8c), proceeding as in (A18) shows that $\tilde{I}_2 = \mathcal{O}(\tau_h - \tau)$.

For \tilde{I}_1 (B8b), we may proceed as in Subsection 7 of Appendix A, using now the asymptotic behavior of \tilde{v} obtained from (B2) to show that the limit $\tau \rightarrow \tau_h$ can be taken under the integral, with the result

$$\begin{aligned} \tilde{I}_1(\omega, \tau, \tau_0) &= \frac{1 - \cos(\omega(\tau_h - \tau_0))}{\omega} + o(1) \\ &= \frac{1 - \cos(\omega\Delta\tau)}{\omega} + o(1). \end{aligned} \tag{B9}$$

Hence

$$J(\omega, \tau, \tau_0) = \frac{1 - \cos(\omega\Delta\tau) + o(1)}{2\pi(\tau_h - \tau)(-\ln(\tau_h - \tau) + \mathcal{O}(1))}. \tag{B10}$$

4. Combining

Adding (B3), (B5), and (B10) gives

$$-\frac{1}{4\pi(\tau_h - \tau)} + \frac{1 + o(1)}{2\pi(\tau_h - \tau)(-\ln(\tau_h - \tau))}, \quad (\text{B11})$$

which gives the result shown in (5.4b).

APPENDIX C: $\dot{\mathcal{F}}$ NEAR THE CAUCHY HORIZON BIFURCATION POINT

In this appendix, we perform the estimates that lead from (5.2) to the results stated in Sec. V for the asymptotics of $\dot{\mathcal{F}}$ near the Cauchy horizon bifurcation point.

The geodesics are those with $E=0$ in (2.18) and (2.19). Proceeding as in Appendix A, we find that (A10) holds but the error term can be improved to

$$\dot{u}(\tau) = \frac{[1 + p((\tau_h - \tau)^2)]}{\kappa_-(\tau_h - \tau)}, \quad (\text{C1})$$

where p is a smooth function of a non-negative argument such that $p(x) = \mathcal{O}(x)$, and similarly for \dot{v} . It follows that the estimate (A11) for $U(\tau_0)/U(\tau)$ improves to

$$\frac{U(\tau_0)}{U(\tau)} = \left(\frac{\tau_h - \tau}{\tau_h - \tau_0}\right)^{\kappa_+/\kappa_-} \times q((\tau_h - \tau)^2), \quad (\text{C2})$$

where q is a smooth positive function of a non-negative argument.

We now need to consider in (A3) and (A4) both the terms that involve \dot{u} and the terms that involve \dot{v} . For the terms that involve \dot{u} , all the estimates given in Appendix A still hold. For the terms that involve \dot{v} , all the estimates given in Appendix B still hold for the Unruh state, while for the HHI state the outcome is the same as with the terms involving \dot{u} , by the left-right symmetry of the state. Combining these observations leads to (5.3b) and (5.4c).

In the Unruh state, the case $\kappa_+/\kappa_- = 2$ is exceptional because the leading term in (5.4c) vanishes due to cancellations. To find the leading term in this case, we need a better estimate for $K(\epsilon, m, \omega)$ (A23) with $A=2$. It is here that we need the improved estimate (C2).

In (A23), setting $A=2$ and isolating the leading behavior gives now

$$K(\epsilon, m, \omega) = K_0(m, \omega) + \epsilon K_1(\epsilon, m, \omega), \quad (\text{C3a})$$

$$K_0(m, \omega) = \int_0^m ds \sin(\omega s) = \frac{1 - \cos(\omega m)}{\omega}, \quad (\text{C3b})$$

$$K_1(\epsilon, m, \omega) = \frac{1}{\tilde{H}(\epsilon)} \int_0^m ds \frac{\sin(\omega s)}{s} \frac{\epsilon s}{\tilde{g}((\epsilon + s)^2) - \tilde{g}(\epsilon^2)}, \quad (\text{C3c})$$

where $\tilde{g}(x) \doteq x/\tilde{H}(\sqrt{x})$ for $x > 0$ and $\tilde{g}(0) \doteq 0$. By the improved estimate (C2), \tilde{g} is smooth and satisfies $\tilde{g}'(x) > 0$ for $x \in [0, \sqrt{R}]$. There thus exists a positive constant k_1 , independent of ϵ , such that $2k_1\epsilon s \leq k_1((\epsilon + s)^2 - \epsilon^2) \leq \tilde{g}((\epsilon + s)^2) - \tilde{g}(\epsilon^2)$ for $s \in [0, m]$ and sufficiently small ϵ . This provides a dominated convergence bound that justifies taking the $\epsilon \rightarrow 0$ limit of $K_1(\epsilon, m, \omega)$ (C3c) under the integral, and the limit is zero. Hence $K(\epsilon, m, \omega) = K_0(m, \omega) + o(1)$ as $\epsilon \rightarrow 0$. This and (B11) give (5.5).

REFERENCES

¹M. Simpson and R. Penrose, *Int. J. Theor. Phys.* **7**, 183 (1973).

²S. W. Hawking and G. F. R. Ellis, *The Large Scale Structure of Space-Time* (Cambridge University Press, Cambridge, UK, 1973).
³R. M. Wald, *General Relativity* (University of Chicago Press, Chicago, 1984).
⁴R. M. Wald, *Quantum Field Theory in Curved Spacetime and Black Hole Thermodynamics* (University of Chicago Press, Chicago, 1994).
⁵R. Brunetti, K. Fredenhagen, and R. Verch, *Commun. Math. Phys.* **237**, 31 (2003).
⁶S. Hollands and R. M. Wald, *Phys. Rept.* **574**, 1–35 (2015).
⁷S. Chandrasekhar and J. B. Hartle, *Proc. R. Soc. London, A* **384**, 301 (1982).
⁸E. Poisson and W. Israel, *Phys. Rev. Lett.* **63**, 1663 (1989).
⁹E. Poisson and W. Israel, *Phys. Rev. D* **41**, 1796 (1990).
¹⁰M. Dafermos, *Contemp. Math.* **350**, 99 (2004).
¹¹M. Dafermos, *Commun. Pure Appl. Math.* **58**, 445 (2005).
¹²J. L. Costa, P. M. Girão, J. Natário, and J. D. Silva, *Commun. Math. Phys.* **339**, 903 (2015).
¹³M. Casals, A. Fabbri, C. Martínez, and J. Zanelli, *Phys. Rev. Lett.* **118**, 131102 (2017).
¹⁴M. Casals, A. Fabbri, C. Martínez, and J. Zanelli, *Phys. Rev. D* **99**, 104023 (2019).
¹⁵S. Hollands, R. M. Wald, and J. Zahn, *Classical Quantum Gravity* **37**, 115009 (2020).
¹⁶S. Hollands, C. Klein, and J. Zahn, *Phys. Rev. D* **102**, 085004 (2020).
¹⁷C. Klein and J. Zahn, *Phys. Rev. D* **104**, 025009 (2021).
¹⁸J. B. Hartle and S. W. Hawking, *Phys. Rev. D* **13**, 2188 (1976).
¹⁹W. Israel, *Phys. Lett. A* **57**, 107 (1976).
²⁰W. G. Unruh, *Phys. Rev. D* **14**, 870 (1976).
²¹B. S. DeWitt, “Quantum gravity: The new synthesis,” in *General Relativity: An Einstein Centenary Survey*, edited by S. W. Hawking and W. Israel (Cambridge University Press, Cambridge, 1979).
²²S. Schlicht, *Classical Quantum Gravity* **21**, 4647 (2004).
²³J. Louko and A. Satz, *Classical Quantum Gravity* **23**, 6321 (2006).
²⁴A. Satz, *Classical Quantum Gravity* **24**, 1719 (2007).
²⁵N. Obadia and M. Milgrom, *Phys. Rev. D* **75**, 065006 (2007).
²⁶J. Louko and A. Satz, *Classical Quantum Gravity* **25**, 055012 (2008).
²⁷B. A. Juárez-Aubry and J. Louko, *Classical Quantum Gravity* **31**, 245007 (2014).
²⁸B. A. Juárez-Aubry, *Int. J. Mod. Phys. D* **24**, 1542005 (2015).
²⁹Y. Décanini and A. Folacci, *Phys. Rev. D* **78**, 044025 (2008).
³⁰P. C. W. Davies, S. A. Fulling, and W. G. Unruh, *Phys. Rev. D* **13**, 2720 (1976).
³¹B. A. Juárez-Aubry and J. Louko, *J. High Energy Phys.* **5**, 140 (2018).
³²S. Y. Lin and B. L. Hu, *Phys. Rev. D* **76**, 064008 (2007).
³³S. Y. Lin, C. H. Chou, and B. L. Hu, *J. High Energy Phys.* **3**, 47 (2016).
³⁴P. Langlois, “Imprints of spacetime topology in the Hawking-Unruh effect,” Ph.D. thesis (University of Nottingham, 2005).
³⁵S. De Bièvre and M. Merkli, *Classical Quantum Gravity* **23**, 6525 (2006).
³⁶S. Kolekar, *Phys. Rev. D* **101**, 025002 (2020).
³⁷H. Bostelmann, C. J. Fewster, and M. H. Rued, *Phys. Rev. D* **103**, 025017 (2021).
³⁸E. Martín-Martínez, T. R. Perche, and B. d L. Torres, *Phys. Rev. D* **103**, 025007 (2021).
³⁹M. H. Rued, *Classical Quantum Gravity* **38**, 195029 (2021).
⁴⁰D. Grimmer, B. de, S. L. Torres, and E. Martín-Martínez, *Phys. Rev. D* **104**, 085014 (2021).
⁴¹E. Martín-Martínez, M. Montero, and M. del Rey, *Phys. Rev. D* **87**, 064038 (2013).
⁴²Á. M. Alhambra, A. Kempf, and E. Martín-Martínez, *Phys. Rev. A* **89**, 033835 (2014).
⁴³A. Raval, B. L. Hu, and J. Anglin, *Phys. Rev. D* **53**, 7003 (1996).
⁴⁴D. J. Raine, D. W. Sciamia, and P. G. Grove, *Proc. R. Soc. A* **435**, 205 (1991).
⁴⁵Q. Wang and W. G. Unruh, *Phys. Rev. D* **89**, 085009 (2014).
⁴⁶P. C. W. Davies and A. C. Ottewill, *Phys. Rev. D* **65**, 104014 (2002).
⁴⁷E. Martín-Martínez and J. Louko, *Phys. Rev. D* **90**, 024015 (2014).
⁴⁸J. Louko, *J. High Energy Phys.* **9**, 142 (2014).
⁴⁹E. G. Brown and J. Louko, *J. High Energy Phys.* **8**, 61 (2015).
⁵⁰L. Thinh, J. D. Bancal, and E. Martín-Martínez, *Phys. Rev. A* **94**, 022321 (2016).
⁵¹D. Moustos, *Phys. Rev. D* **98**, 065006 (2018).

- ⁵²J. Louko, *Classical Quantum Gravity* **35**, 205006 (2018).
- ⁵³W. Cong, E. Tjoa, and R. B. Mann, *J. High Energy Phys.* **6**, 21 (2019); erratum, **7**, 51 (2019).
- ⁵⁴E. Tjoa and E. Martín-Martínez, *Phys. Rev. D* **101**, 125020 (2020).
- ⁵⁵E. Tjoa and R. B. Mann, *J. High Energy Phys.* **8**, 155 (2020).
- ⁵⁶N. K. Kollas and D. Moustos, *Phys. Rev. D* **105**, 025006 (2022).
- ⁵⁷D. Hümmer, E. Martín-Martínez, and A. Kempf, *Phys. Rev. D* **93**, 024019 (2016).
- ⁵⁸L. Hörmander, *The Analysis of Linear Partial Differential Operators* (Springer, Berlin, 1986).
- ⁵⁹C. J. Fewster, *Classical Quantum Gravity* **17**, 1897 (2000).
- ⁶⁰See <http://dlmf.nist.gov/> for “NIST Digital Library of Mathematical Functions, Release 1.1.2,” accessed 15 June, 2021.
- ⁶¹R. M. Wald, *Ann. Phys.* **110**, 472 (1978).
- ⁶²N. D. Birrell and P. C. W. Davies, *Quantum Fields in Curved Space* (Cambridge University Press, Cambridge, UK, 1982).
- ⁶³S. Takagi, *Prog. Theor. Phys. Suppl.* **88**, 1 (1986).
- ⁶⁴L. J. Romans, *Nucl. Phys. B* **383**, 395 (1992).
- ⁶⁵E. Winstanley and P. M. Young, *Phys. Rev. D* **77**, 024008 (2008).
- ⁶⁶K. K. Ng, C. Zhang, J. Louko, and R. B. Mann, “A little excitement across the Horizon,” [arXiv:2109.13260](https://arxiv.org/abs/2109.13260) (2021).
- ⁶⁷A. Conroy and P. Taylor, “Response of an Unruh-DeWitt detector near an extremal black hole,” [arXiv:2109.04486](https://arxiv.org/abs/2109.04486) (2021).
- ⁶⁸E. Ayon-Beato and A. Garcia, *Phys. Lett. B* **464**, 25 (1999).
- ⁶⁹R. Gambini, E. M. Capurro, and J. Pullin, *Phys. Rev. D* **91**, 084006 (2015).